J. of Supercritical Fluids 63 (2012) 187–198

Contents lists available at SciVerse ScienceDirect

The Journal of Supercritical Fluids

journal homepage: www.elsevier.com/locate/supflu

Mechanism of extensional stress-induced cell formation in polymeric foaming processes with the presence of nucleating agents

Siu N. Leung, Anson Wong, Lilac Cuiling Wang, Chul B. Park*

Microcellular Plastics Manufacturing Laboratory, Department of Mechanical and Industrial Engineering, University of Toronto, Toronto, Ontario, Canada M5S 3G8

ARTICLE INFO

Article history:
Received 29 August 2011
Received in revised form
12 December 2011
Accepted 14 December 2011

Keywords:
Cell nucleation
Critical radius
Extensional stress
Nucleating agents
Polymeric foaming processes
Pre-existing gas cavities

ABSTRACT

Addition of nucleating agents (e.g., talc) is a common way to promote the cell density in polymeric foaming process. It is widely believed that such enhancement is caused by the decrease in free energy barrier for the nucleation to initiate heterogeneously as well as the reduction in gas loss with the existence of the inorganic fillers. In this paper, *in situ* visualization of the cell formation phenomena during polymeric foaming processes of polystyrene–talc composites blown with carbon dioxide revealed that the expansion of nucleated cells triggered the formation of secondary cells around them. Subsequently, the expansion of the secondary cells also promoted the formation of tertiary cells around them similar to a chain reaction. These observations provided evidences to support the theoretical simulation of stress-induced cell formation around expanding bubbles. A series of parametric studies were conducted to correlate the stress-induced cell formation and various processing and material parameters. The elucidation of the aforementioned cell formation mechanism with the presence of nucleating agents would provide additional guidelines for polymeric foam manufacturers to control the cell morphologies of their products in order to optimize and tailor the desired physical properties.

1. Introduction

Heightened needs for light-weight materials with improved cushioning, insulating, structural performance and other characteristics are expected to increase the world demand for polymeric foams. Extensive research has proven that plastic foams with high cell densities, small cell sizes, and narrow cell-size distributions can translate into notable advantages in various applications. Compared with their solid counterparts, polymeric foams with high cell density and uniform cell sizes have superior mechanical properties, including toughness [1], impact strength [2–4], fracture strength [4], and fatigue life [5]. Moreover, foams with tailored cell morphologies can offer improved thermal insulation [6,7], enhanced acoustical insulation [7], and desired optical properties [8]. Given these and other findings, it seems the possibilities are virtually endless. However, the complete control of the functional properties of polymeric foams hinges on the ability to precisely control of cellular morphology including cell number density, void fraction, and open- versus closed-cell structures.

During polymeric foaming processes, nucleating agents, such as inorganic fillers (e.g., talc particles), organic phrases (e.g., elastomer phases), and nanoparticles (e.g., nanoclay and carbon nanotubes), are commonly used to facilitate the control of cellular structures and to produce high-quality foam products. Various research groups have investigated the effects of different nucleating agents on polymeric foaming processes. In the 1960s, Hansen et al. [9,10] carried out a pioneer exploration of the effects of nucleating agents on cell nucleation. As an extension of their work, a series of studies identified effective nucleating agents for producing plastic foams, including azodicarbonamide [11], calcium carbonate [11,12], calcium stearate [11,13], magnesium silicate [14], sodium benzoate [11,15], stearic acid [16], silica products [11,12,17], talc [11,18–20], and zinc stearate [11–17]. In the past decade, nanocomposite foams have received considerable attention in both academic research and industrial investigation, and nanotechnology is continuing to evolve. During nanocomposite foaming, nano-sized particles work as heterogeneous nucleating sites to promote cell nucleation. Recent studies have demonstrated that nanoparticles (e.g., nanoclay [21–24], carbon nanofibers [25], and single-walled carbon nanotubes [25]) could result in higher cell density in plastic foams. These studies attribute the promotion of heterogeneous cell nucleation to the extremely fine dimensions and large total surface area of nucleating agents. They also note that special properties, such as better fire retardance, improved barrier resistance, and higher thermal insulation, can be achieved by selecting appropriate, or a combination of, nanoparticles [26,27].

From a thermodynamic perspective, the energy barrier to initiate heterogeneous nucleation on a flat surface was investigated by Turnbull and Vonnegut [28]. The concept was extended to curved

* Corresponding author. Tel.: +1 416 978 3053; fax: +1 416 978 0947.
E-mail addresses: leungsun@mie.utoronto.ca, leungsun@rogers.com (S.N. Leung), park@mie.utoronto.ca (C.B. Park).

0896-8446/$ – see front matter © 2011 Elsevier B.V. All rights reserved.
doi:10.1016/j.supflu.2011.12.018

surfaces by Fletcher [29] and to rough surfaces by Cole [30]. In each case, classical thermodynamics were employed to prove that the free energy barrier to heterogeneously nucleate a bubble is less than that required to nucleate a cell homogeneously. The amount of energy reduction depends on the geometry of the interfaces between the polymer and the nucleating agents, and on the interfacial energies. In this context, Leung et al. [31] demonstrated that the surface geometry of a heterogeneous nucleating site is a critical factor for governing the final cell density and cell size distribution. Recently, Wang et al. [32] numerically simulated the pressure profile in the vicinity of nucleating agents near an expanding bubble. The study revealed that the expansion of nucleated cells would generate local flow fields that induce tensile stresses around nearby particles (e.g., talc), resulting in local pressure fluctuations that enhance additional cell formation. This provides new information about the underlying mechanism that promotes cell nucleation in the presence of cell nucleating agents.

To improve foaming technologies and products, extensive research has been done to elucidate the effect of nucleating agents on cell nucleation. Extrusion foaming experiments of various polymers using different blowing agents [18–20] showed that cell densities increased with talc content in most cases. These investigations highlighted two additional facts. Firstly, regardless of the types of blowing agents, further addition of talc particles beyond 10 wt% had a negligible effect on the cell density when compared to cases with lower talc contents [18]. Park et al. speculated that the agglomeration of talc particles at high loading did not create substantially more nucleating sites and led to the negligible effect of further increasing the talc content on cell density. Secondly, when CO_2 was used as the blowing agent, the correlation between the talc content and the final cell density was less apparent [18,20], especially at a high CO_2 concentration (e.g., 5 wt%). In this content, Lee proposed that the increase in cell density by adding nucleating agents might relate to the shear-induced nucleation [33]. Since stress is a key factor in polymeric foaming processes, different researchers had attempted to investigate its effects in a more controlled environment by *in situ* observing continuous foaming processes in foam extrusion systems through transparent slit dies [34–37]. These studies concluded that the combined effect of extensional and shear stresses promoted cell nucleation. However, because the cell nucleation and growth phenomena occurred in a highly coupled environment that involved complex thermodynamic, fluid mechanic, and rheological processes, they were difficult to be thoroughly understood. In this context, other researchers developed batch foaming systems that induced shear stresses [38,39] or a combination of them and vibrations [40]. These studies aimed to identify the criteria for stress states that favor plastic foaming for optimizing die design and mold plastic foaming equipment. As an extension of the pioneer research on stress-induced polymeric foaming processes, Wong et al. developed a novel visualization system to explore the effects of extensional stress/strain on foaming behaviors of polymer materials [41].

Most previous theoretical studies accounted for the promotion of heterogeneous cell nucleation by adding talc particles or other nucleating agents as the combined result of a reduction in the free energy barrier to nucleate cells and an increase in the number of heterogeneous nucleating sites. In this context, Lee also speculated that the energy associated with the shear work in polymer flow helps to overcome the energy barrier, thus promoting cell nucleation [33]. Moreover, Wang et al. numerically analyzed the pressure profile in the vicinity of nucleating agents and suggested that growing cell would induce a pressure fluctuation around the particulates, which is tensile in nature and promote the cell formation [32].

This paper aims to elucidate the hypothesis on the stress-induced nucleation made by Lee [33] as well as to provide experimental evidence to support the numerical simulation of the stress-induced nucleation conducted by Wang et al. [32]. The foaming of polystyrene–talc (PS–talc) compounds using carbon dioxide (CO_2) as the physical blowing agent is taken as a case study. A series of batch foaming experiments were conducted using a visualization system [42] to observe the *in situ* foaming behaviors of PS and PS–talc compounds being blown by CO_2. The observed changes in cell nucleation behaviors with the presence of talc particles are discussed using the concept of critical radius, taking into account the effects of sizes, contents, and types of talc particles, the blowing agent contents, and the processing temperatures. The results would provide additional guidelines for manufacturers of polymeric foam products to choose the ideal nucleating agents and optimize their processes as well as for nucleating agent supplier to improve their products.

2. Theoretical framework

The batch foaming experiments described herein investigated a polymeric foaming process utilizing an isothermal decompression of a saturated polymer–inorganic filler–gas system (e.g., PS–talc–CO_2). Within the pressure chamber, the plastic foam was allowed to expand freely. Based on the classical nucleation theory [43], a critical bubble with its radius equal to the critical radius (R_{cr}) is at an unstable equilibrium state with its surroundings. Using classical thermodynamics, it can be derived that R_{cr} is a function of dissolved gas concentration (C), system pressure (P_{sys}), and system temperature (T_{sys}), which is expressed as

$$R_{cr} = \frac{2\gamma_{lg}}{P_{bub,cr} - P_{sys}} \tag{1}$$

where γ_{lg}, the interfacial energy at the liquid–gas (i.e., PS–CO_2) interface, and $P_{bub,cr}$, the pressure inside a critical bubble, are both functions of C, P_{sys}, and T_{sys}. In order to minimize the free energy, nuclei or bubbles that are larger than R_{cr} grow spontaneously, whereas those that are smaller than R_{cr} collapse. Tucker and Ward experimentally verified this concept and examined the stability of bubbles in an unsaturated water-oxygen solution [44]. Similarly, during plastic foaming, nuclei or bubbles that are larger than R_{cr} can sustain and expand, while those that are smaller than R_{cr} shrink and disappear [45].

The classical nucleation theory is derived from continuum thermodynamics and does not consider any discontinuity in the thermodynamic system. According to the theory, the main driving force for cell nucleation is the degree of supersaturation (ΔP), which can be expressed as

$$\Delta P = P_{bub,cr} - P_{sys} \tag{2}$$

The free energy change for forming a bubble homogeneously, W_{hom}, and a bubble heterogeneously, W_{het}, can be expressed, respectively, as [46–49]

$$W_{hom} = \frac{16\gamma_{lg}^3}{3\left(P_{bub,cr} - P_{sys}\right)^2} \tag{3}$$

$$W_{het} = \frac{16\gamma_{lg}^3 F\left(\theta_c, \beta\right)}{3\left(P_{bub,cr} - P_{sys}\right)^2} = W_{hom} F\left(\theta_c, \beta\right) \tag{4}$$

where $F(\theta_c, \beta)$ is an energy reduction factor. Physically, it is the ratio of the volume of a cell nucleated on the heterogeneous nucleating agent (e.g., talc) to that of a spherical cell with the same radius but nucleated homogeneously. In other words, it depends on both the interfacial properties of the liquid–gas, solid–gas, and solid–liquid interfaces, and the surface geometry of the heterogeneous nucleating sites [31].

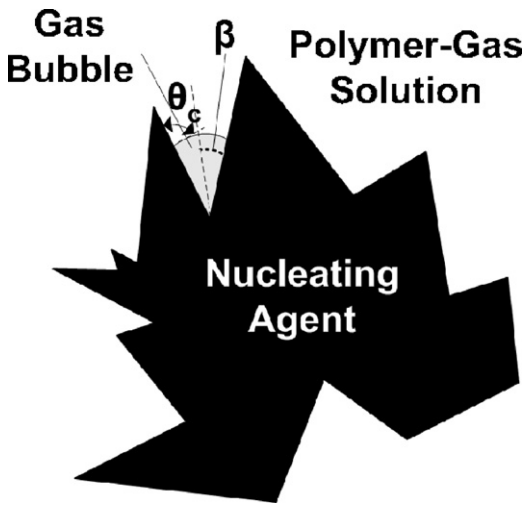

Fig. 1. A nucleating agent or its agglomerate.

Table 1
Physical properties of polystyrene.

	PS685D
MFI	1.5 g/10 min
M_n	120 000
M_w/M_n	2.6
Specific gravity	1.04
Glass transition temperature (T_g)	108 °C

Table 2
Properties of talc particles.

Name of talc	Mean size (μm)	Surface treatment
Cimpact 710	1.7	No
CB7	1.8	Yes
Stellar 410	10.0	No

In typical plastic foaming processes, nucleating agents are used to enhance the control of the foam structures. For inorganic fillers, such as talc, particles tend to aggregate together to form agglomerates [33]. Therefore, the surfaces of the heterogeneous nucleating sites are rough and can be modeled as a series of conical cavities, as indicated in Fig. 1. The energy reduction factor, $F(\theta_c, \beta)$, can be derived as [30,50]

$$F(\theta_c, \beta) = \frac{1}{4}\left\{2 - 2\sin(\theta_c - \beta) + \frac{\cos\theta_c \cos^2(\theta_c - \beta)}{\sin\beta}\right\} \quad (5)$$

Blander and Katz suggested that the homogeneous nucleation rate (J_{hom}) and the heterogeneous nucleation rate (J_{het}) are equivalent to the rate at which the critical bubbles gain molecules and grow [51]. Combining the classical nucleation theory and

Table 3
Physical properties of the blowing agent.

	Carbon dioxide
Chemical formula	CO_2
Molecular weight	44.01 g mol
Sublimation point	−78.45 °C
Critical temperature	31.05 °C
Critical pressure	7.38 MPa

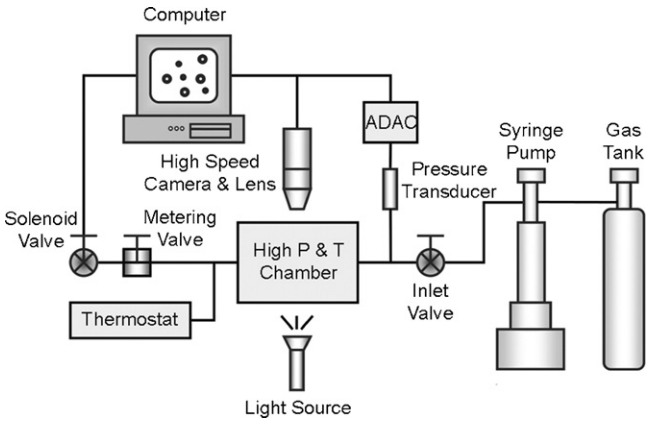

Fig. 2. The Batch Foaming Visualization System [42].

molecular kinetics, the expressions for J_{hom} [51] and J_{het} [52] are derived as

$$J_{hom} = N\sqrt{\frac{2\gamma_{lg}}{\pi m}\exp\left(-\frac{W_{hom}}{k_B T_{sys}}\right)} \quad (6)$$

$$J_{het} = \int_\beta \rho_\beta(\beta) N^{\frac{2}{3}} Q(\theta_c, \beta)\sqrt{\frac{2\gamma_{lg}}{\pi m F(\theta_c, \beta)}\exp\left(-\frac{W_{het}}{k_B T_{sys}}\right)}\,d\beta \quad (7)$$

where N is the number of gas molecules per unit volume of unfoamed polymer; m is the mass of a gas molecule; k_B is the Boltzmann's constant; $\rho_\beta(\beta)$ is the probability density function to represent the randomness of the size of β; and $Q(\theta_c, \beta)$ is the ratio of the liquid–gas interfacial area of a cell nucleated on the heterogeneous nucleating agent (e.g., talc) to that of a cell with the same radius but nucleated homogeneously. $Q(\theta_c, \beta)$ is expressed as [30]

$$Q(\theta_c, \beta) = \frac{1 - \sin(\theta_c - \beta)}{2} \quad (8)$$

Experimental observations of plastic foaming revealed that foam appears at low supersaturation levels where no nucleation should occur according to the calculation based on Eq. (6) [19]. This suggests that nucleation is heterogeneous in typical polymeric foaming processes. The total number of nucleated cells per unit unfoamed volume of polymer, $N_b(t)$, within a time period, t, can be estimated by

$$N_b(t) = \int_0^t J_{hom}(t') + A_{het}(t') J_{het}(t')\,dt' \approx \int_0^t A_{het}(t') J_{het}(t')\,dt' \quad (9)$$

Although continuum thermodynamics has provided numerous insights on the cell nucleation process during plastic foaming, it does not adequately describe the real situation. Furthermore, a nucleating agent or its agglomerates (i.e., talc particles) may have rough or porous surfaces, and would not be totally wetted by the viscous polymer melt [53]. Therefore, the polymer–filler interfaces provide extra crevices for gas molecules to accumulate to become pre-existing gas cavities. During plastic foaming, the pre-existing gas cavities hidden at the polymer–filler interfaces can serve as seeds for bubble formation. However, practically, the activation energy for homogeneous nucleation is much higher than that of heterogeneous nucleation, and therefore, in most cases, heterogeneous nucleation will be dominant [33,54,55]. The expansion of these pre-existing gas cavities depends on the dynamic change of R_{cr} during a foaming process. At the beginning of the process, a

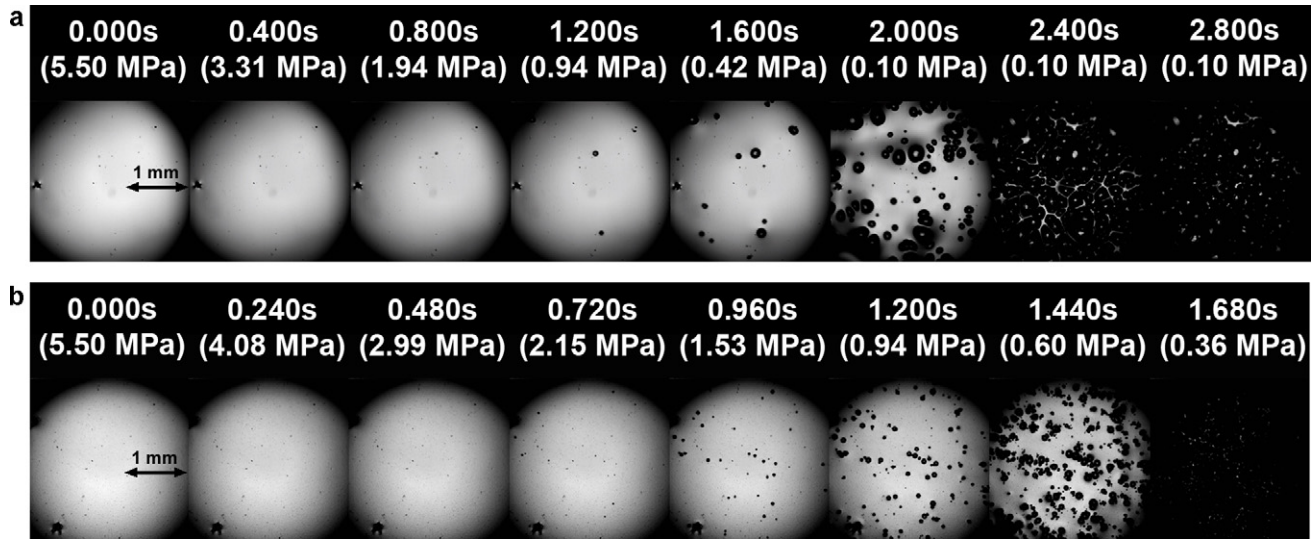

Fig. 3. Micrographs of PS foaming with 2.1 wt% CO_2 at 180 °C: (a) pure PS and (b) PS + 5 wt% talc (CIMPACT 710).

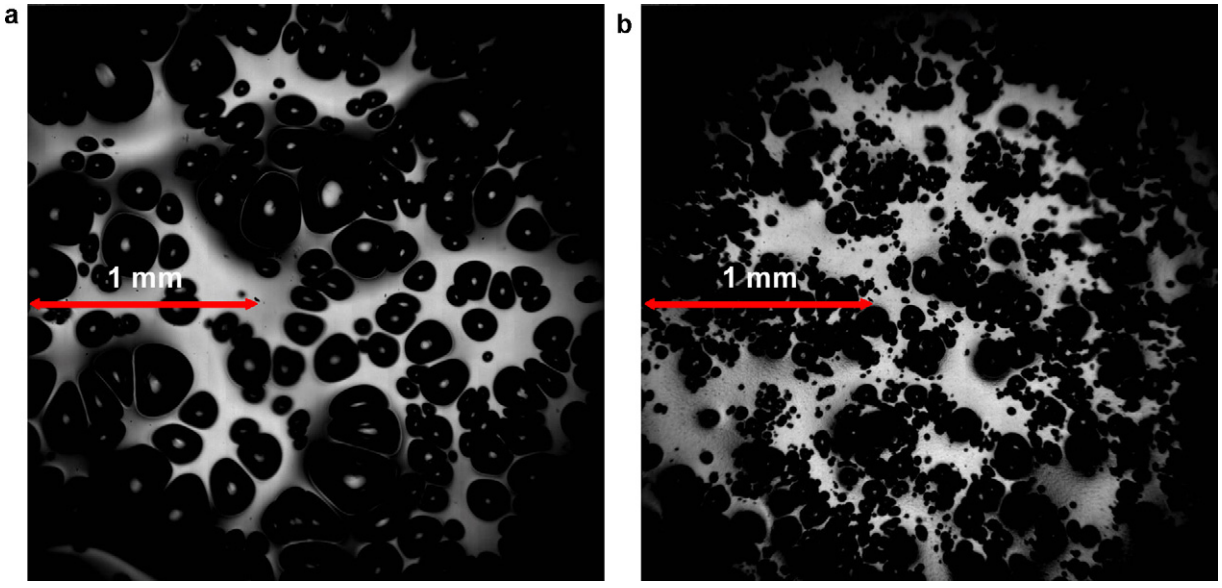

Fig. 4. Micrographs of PS foaming with 2.1 wt% CO_2 at 180 °C: (a) pure PS at 2.20 s (0.10 MPa) and (b) PS + 5 wt% talc (CIMPACT 710) at 1.56 s (0.47 MPa).

rapid system pressure drop dramatically increases ΔP, leading to a significant reduction in R_{cr} according to Eq. (1). Once R_{cr} becomes smaller than the radii of curvatures of the pre-existing cavities, these seeds are activated and start to grow into cells in the polymer matrix. Upon bubble expansion, R_{cr} starts to increase due to the gas depletion around the growing bubble. If R_{cr} becomes larger than the bubbles' radii (R_{bub}) due to extensive gas depletion, these bubbles will shrink and collapse.

During the rapid system pressure drop in the foaming processes, it is expected that pressure fluctuation exists in different regions of the matrix. Wang et al. [32] numerically simulated such pressure fluctuation is significant in the vicinity of the regions where

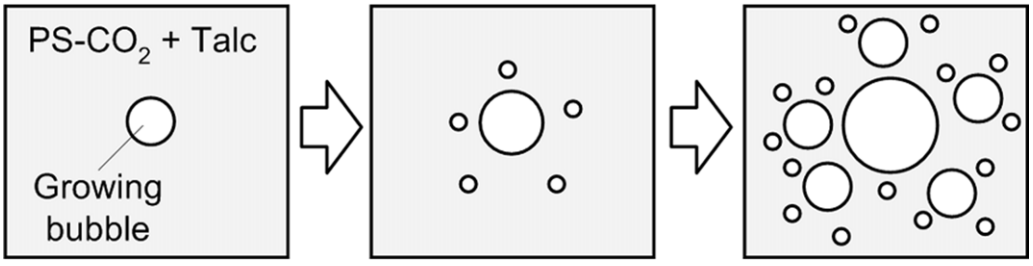

Fig. 5. Schematics of the bubble formation phenomena.

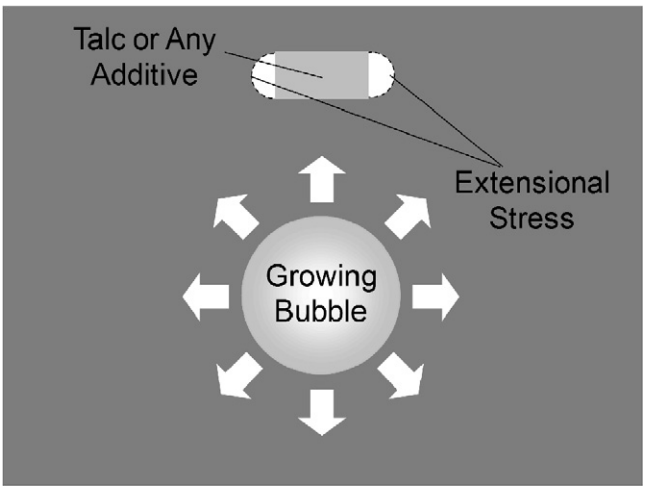

Fig. 6. A schematic of the extensional stress field around the talc agglomerate induced by the expanding bubble [32].

cells are expanding near nucleating agent particulates. To account for the local pressure fluctuation, the expression for the degree of supersaturation (ΔP) can be rewritten as

$$\Delta P = P_{bub,cr} - \left(P_{sys} + \Delta P_{local}\right) \tag{10}$$

where ΔP_{local} is the difference between P_{sys} in the bulk and the actual pressure at the nucleating site. If the local region experiences a compressive stress, ΔP_{local} will be positive. In contrast, if the local region is under an extensional stress, ΔP_{local} will be negative. As a result, Eqs. (1), (3), and (4) become

$$R_{cr} = \frac{2\gamma_{lg}}{P_{bub,cr} - \left(P_{sys} + \Delta P_{local}\right)} \tag{11}$$

$$W_{hom} = \frac{16\gamma_{lg}^3}{3\left(P_{bub,cr} - \left(P_{sys} + \Delta P_{local}\right)\right)^2} \tag{12}$$

$$W_{het} = \frac{16\gamma_{lg}^3 F\left(\theta_c, \beta\right)}{3\left(P_{bub,cr} - \left(P_{sys} + \Delta P_{local}\right)\right)^2} = W_{hom} F\left(\theta_c, \beta\right) \tag{13}$$

According to Eqs. (11)–(13), if there is an extensional stress at the local region (i.e., $\Delta P_{local} < 0$), W_{hom}, W_{het}, and R_{cr} will all decrease. In contrast, if there is a compressive stress at the local region (i.e., $\Delta P_{local} > 0$), W_{hom}, W_{het}, and R_{cr} will all increase. The views of the classical thermodynamics on cell nucleation argue that any local extensive stress will reduce the free energy barriers for both homogeneous nucleation and heterogeneous nucleation, and the cell nucleation rate will be higher because of the promotion of the heterogeneous nucleation. On the other hand, considering cells grow from the pre-existing gas cavities at the polymer–filler interfaces, the increase in ΔP leads to a more rapid decrease in R_{cr} and an earlier activation of the pre-existing gas cavities to form cells. Therefore, it is critical for academic and industrial research to explore the factors affecting the local pressure field. The resulting knowledge will provide alternative processing strategies to optimize and tailor foam morphology for various applications.

3. Experimental

3.1. Materials

The polymer matrix material for the PS–talc compounds described here is Styron 685D polystyrene with a weight-average molecular weight of 315 000 g/mol (The Dow Chemical Co.). The manufacturer reports that no specific nucleating agents were added to PS 685D. The three types of talc particles, Cimpact 710, CB7, and Stellar 410 (Luzenac), used for the experimental work differ in either mean particle size or surface treatment. The physical blowing agent used for the foaming experiments was 99% pure CO_2 (Linde Gas). The physical properties of the polymer, talc particles, and blowing agent are summarized in Tables 1–3.

3.2. Sample preparation

For each of the three types of talc particles, a 20 wt% of talc masterbatch of PS was prepared using a C.W. Brabender 3-piece mixer. Each masterbatch was diluted with pure PS, using the same batch mixer to produce PS–talc compounds with talc contents of 0.5, 1.0, 2.0, and 5.0 wt%. For the neat PS used in the control experiments, the resins, without the addition of talc particles, were processed by the batch mixer following the aforementioned procedures to ensure the same processing history as that experienced by the PS–talc compounds. Next, a compression molding machine (Carver Inc.) equipped with a digital temperature controller was used to prepare film samples of the PS and PS–talc compounds. Neat PS or PS–talc compounds were hot compression-molded into

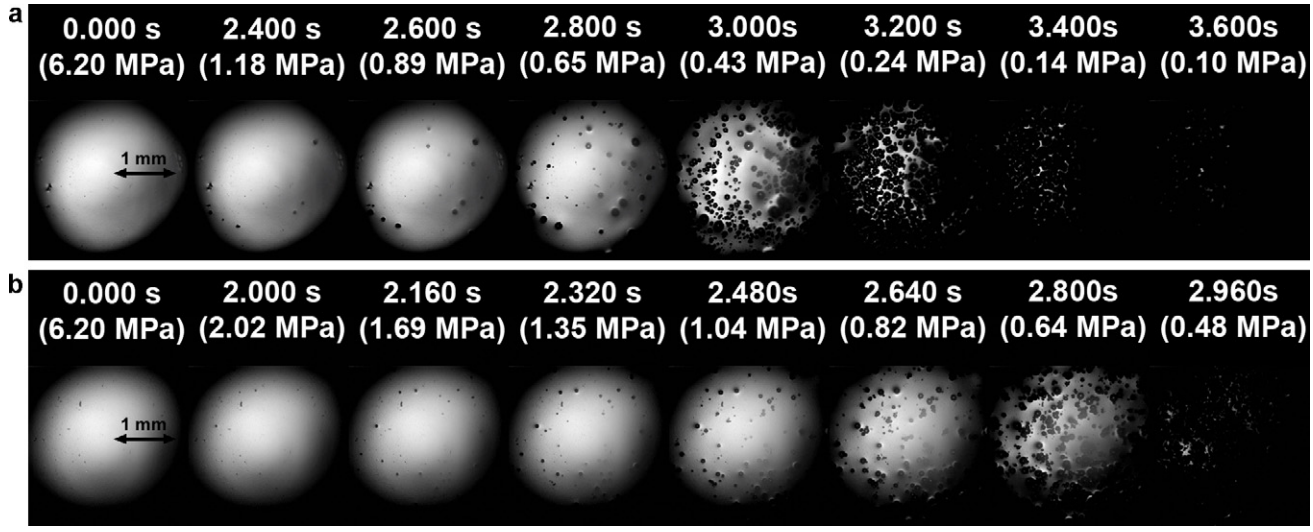

Fig. 7. Micrographs of PS with 2.3 wt% CO_2 at 180 °C: (a) PS + 0.5 wt% talc (CIMPACT 710) and (b) PS + 5 wt% talc (CIMPACT 710).

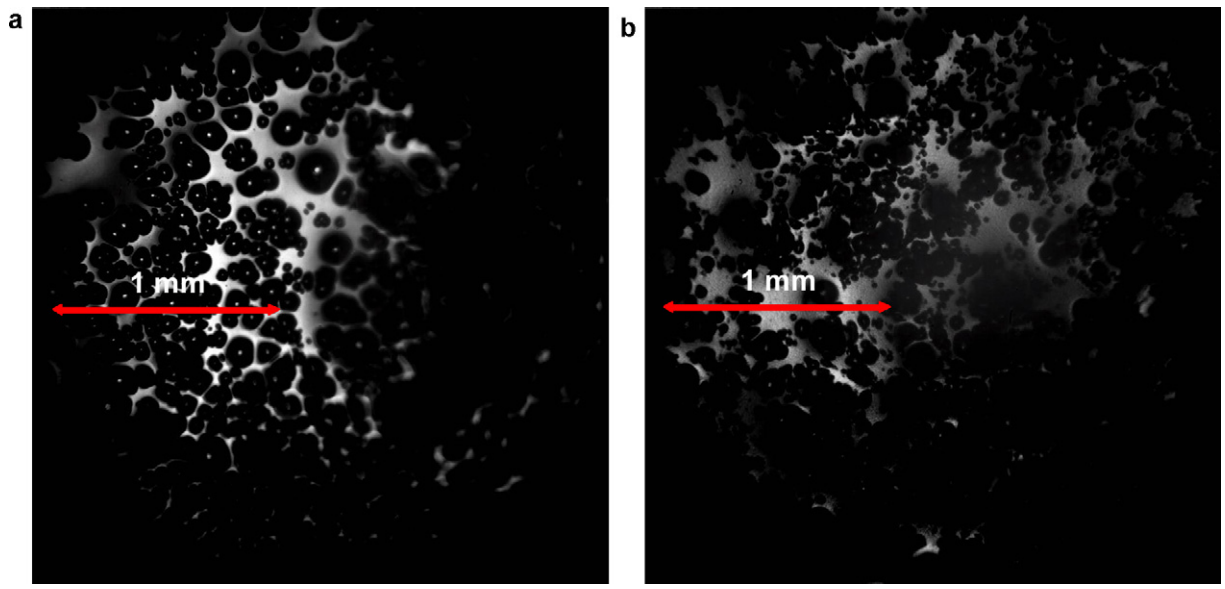

Fig. 8. Micrographs of PS foaming with 2.3 wt% CO_2 at 180 °C: (a) PS + 0.5 wt% talc (CIMPACT 710) at 3.20 s (0.24 MPa) and (b) PS + 5 wt% talc (CIMPACT 710) at 2.90 s (0.53 MPa).

200 μm thick films using the press, which was pre-heated to a temperature above the glass transition temperature of PS. The PS and PS–talc films were then punched into disc-shaped samples of about 6 mm in diameter for the foaming visualization experiments.

3.3. *In situ* foaming visualization

The setup of the batch foaming visualization system [42], as illustrated in Fig. 2, was used to observe the *in situ* foaming behavior of the aforementioned polymer–blowing agent system. The system consists of a high-pressure, high-temperature chamber, a pressure-drop rate control system, a data acquisition system for pressure measurement (i.e., a data acquisition board and a computer), a gas supply system (i.e., a gas tank, a syringe pump, and valves), and an optical system (i.e., an objective lens, a light source, and a high-speed CMOS camera). With a maximum frame rate of 120 000 frames per second, the CMOS camera is capable of capturing plastic foaming processes with high temporal resolution.

The foaming experiments were performed according to the following steps:

STEP 1: The chamber loaded with the PS or PS–talc sample was charged with CO_2 at the pre-determined saturation pressure, and the chamber temperature was controlled using a thermostat.
STEP 2: The pressure and temperature of the chamber were maintained at the set points for 30 min to allow the sample to be saturated with CO_2.
STEP 3: CO_2 was released by opening the solenoid valve. The pressure transducer and the CMOS camera captured the pressure decay data and *in situ* foaming data, respectively. The opening of the solenoid valve and the data capturing were synchronized by two computers and the data acquisition system.

A number of experiments were conducted to explore the effects of talc on the cell nucleation mechanism of the PS–CO_2 system. Processing conditions and material parameters were altered to take into account the effects of sizes,

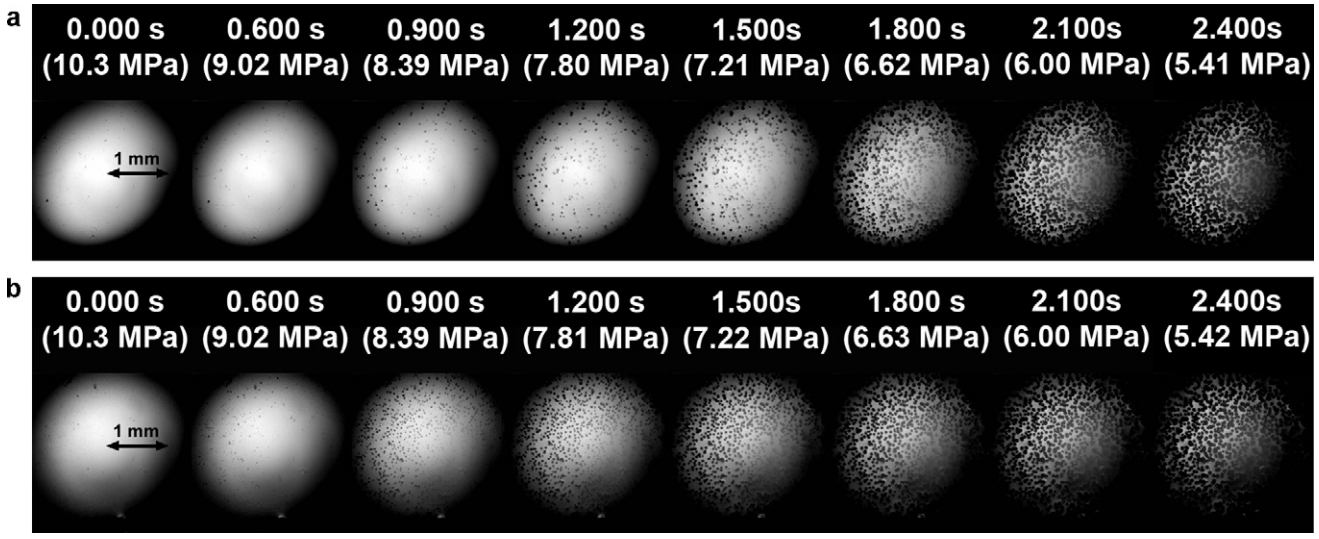

Fig. 9. Micrographs of PS with 4.0 wt% CO_2 at 180 °C: (a) PS + 0.5 wt% talc (CIMPACT 710) and (b) PS + 5 wt% talc (CIMPACT 710).

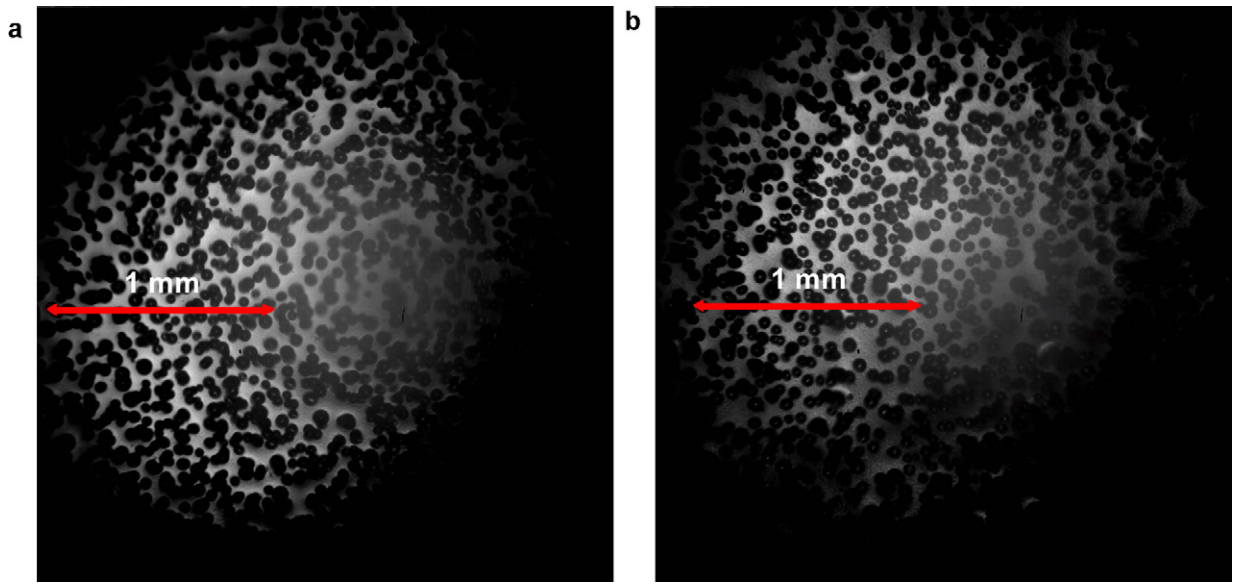

Fig. 10. Micrographs of PS foaming with 4.0 wt% CO_2 at 180 °C: (a) PS + 0.5 wt% talc (CIMPACT 710) at 2.40 s (5.41 MPa) and (b) PS + 5 wt% talc (CIMPACT 710) at 2.40 s (5.42 MPa).

contents, and types of talc particles, the blowing agent contents, as well as the processing temperatures on the nucleation mechanism. As control experiments, the foaming phenomena of pure PS samples, which underwent the same processing history as the PS–talc samples, were captured and compared with the visualization data of the PS–talc–CO_2 foaming experiments.

3.4. Characterization

To gain insight into the effect of the surface treatment of talc particles on their dispersion in the polymer matrix, the cross-sections of the PS–talc composites were analyzed using scanning electron microscopy (SEM) to investigate the distribution of talc particles along the thickness direction. All PS–talc samples were fractured

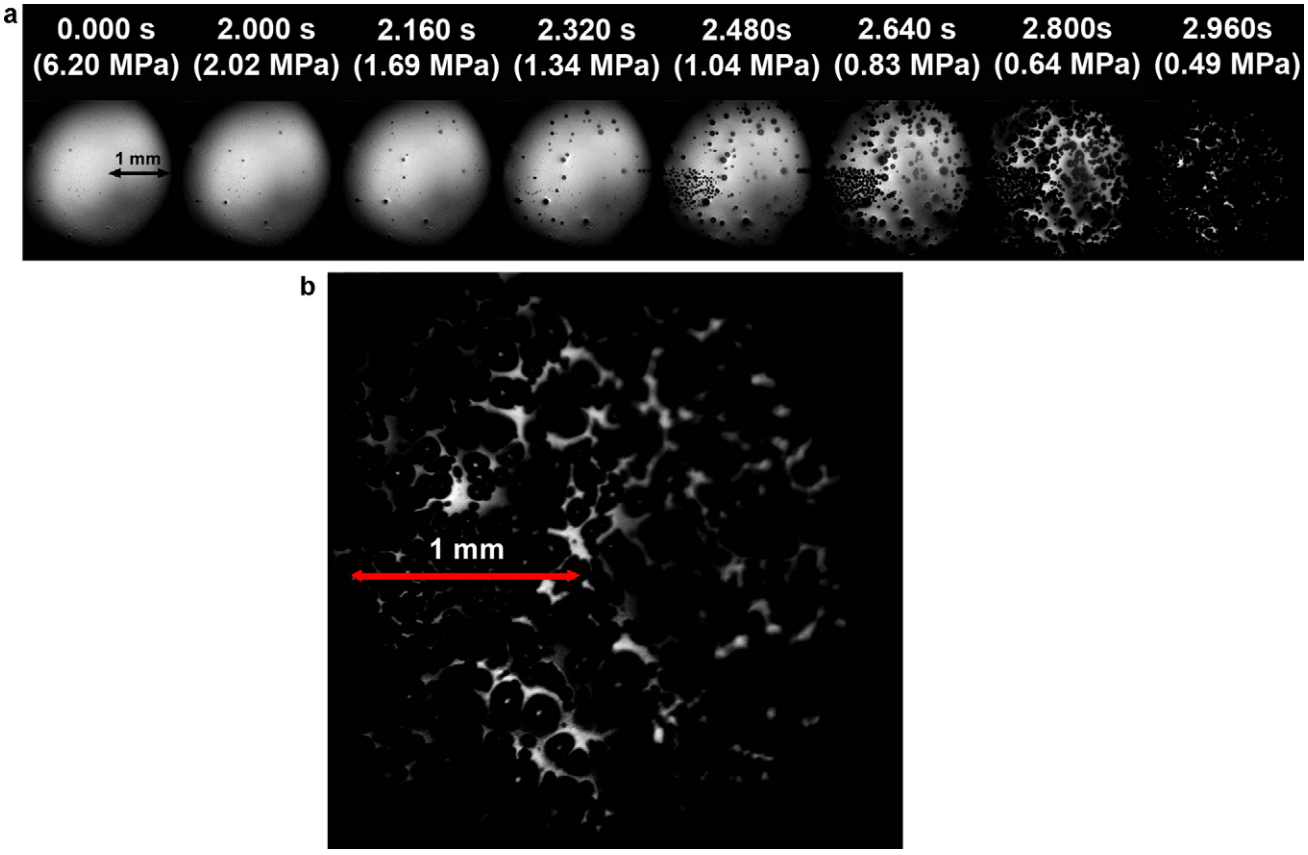

Fig. 11. Micrographs of PS + 5.0 wt% talc (CB7) with 2.3 wt% CO_2 at 180 °C: (a) until 2.96 s (0.49 MPa) and (b) at 2.88 s (0.57 MPa).

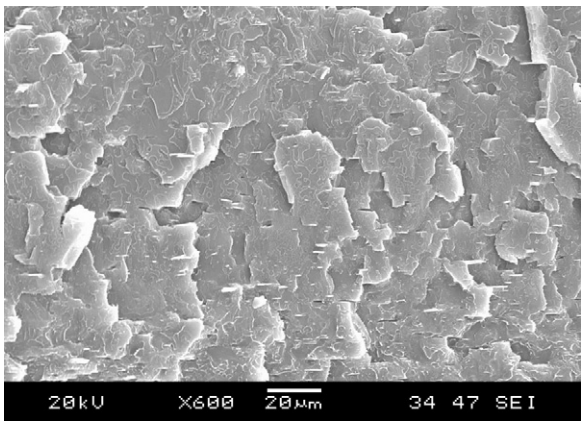

Fig. 12. A SEM micrograph of PS + 5 wt% talc (CB7).

in liquid nitrogen and their cross-sections were studied using SEM (JEOL, model JSM-6060).

4. Results and discussion

4.1. Effect of talc particles on cell nucleation

A pure PS disk sample and a PS–talc composite disk sample, which consisted of 5 wt% of talc loading (i.e., CIMPACT 710), were pressurized to 5.5 MPa at 180 °C. After complete saturation, 2.1 wt% of CO_2 [56] was dissolved in each sample. These samples were then foamed by rapid depressurization with similar pressure drop profiles; Fig. 3(a) and (b) shows the micrographs of their *in situ* foaming phenomena. With the presence of 5 wt% of untreated talc particles, the onset time of cell nucleation was earlier, and the cell density increased dramatically. These results indicate that talc serves as an effective heterogeneous nucleating agent during the foaming process, a finding consistent with previous studies [18–20]. The observations can be explained in two different perspectives. According to the classical nucleation theory, the presence of talc would lower the free energy barrier to nucleate cells. Therefore, a lower degree of supersaturation was required to nucleate new cells, which led to earlier cell nucleation. On the other hand, if cell formation started from the pre-existing cavities, during the rapid pressure decay, R_{cr} would continuously reduce, ultimately becoming smaller than the radii of the pre-existing CO_2 cavities that were ubiquitous on the rugged surfaces of talc agglomerates [33]. Subsequently, these cavities would be activated and begin to grow. The omnipresence of CO_2 cavities, together with the lower free energy barrier for cell nucleation, enhanced cell formation and resulted in higher cell density.

In addition to the typical effects of talc on cell nucleation, a counter-intuitive phenomenon was observed in the visualization experiments. Fig. 4(a) and (b) indicates that during the foaming of the PS–talc sample, new cells were generated near the previously nucleated and growing cells despite the rapid gas consumption by cell growth in these regions. This phenomenon was less pronounced when the pure PS sample was foamed. Fig. 5 illustrates the schematics of the observed bubble formation phenomenon in the PS–talc sample. The *in situ* observation offers insight into the underlying mechanism of talc-enhanced nucleation, thus permitting a more complete explanation of the mechanism by which inorganic fillers promote heterogeneous cell nucleation. The observed phenomena also served as evidence to support the numerically simulated pressure profile in the vicinity of expanding bubbles near nucleating agent particulates by Wang et al. [32]. Using the simulated results of local pressure fluctuation [32], the observed pressure drop to initiate cell formation, together with Eqs. (12)–(13), and it can be estimated that the free energy barrier for both homogeneous and heterogeneous nucleation would be reduced. This would result in the promoted cell formation around the expanding bubbles.

As nucleated bubbles expand, their growth will induce tangential stretching actions on their surfaces and generate flow fields in the surrounding polymer–gas solution. The cell growth will reduce the cell wall thickness, bringing the talc aggregates and the polymer–gas solution towards the growing bubble. Fig. 6 shows a schematic to illustrate the generation a local pressure fluctuation around the side surfaces of the talc agglomerate by the extensional flow. This local pressure field is tensile and will result in a negative ΔP_{local}. Using Eqs. (11)–(13), it can be deduced that R_{cr}, W_{hom}, and W_{het} will all be reduced, promoting the nucleation of new cells as well as the growth of pre-existing gas cavities, and eventually increasing the cell density of the plastic foam.

4.2. Effect of talc content on cell nucleation

By varying the talc (CIMPACT 710) loading from 0.5 to 5.0 wt%, a series of batch foaming experiments were conducted to investigate the effect of talc content on the cell nucleation phenomena. In the experiments, all PS–talc composite samples were foamed with CO_2 at 180 °C with similar pressure drop profiles. Since previous studies revealed that increasing the talc content will enhance cell formation to different extents as the dissolved CO_2 content varies [18,20], the effect of talc content on the PS–talc foaming behaviors was examined under two CO_2 concentrations, 2.3 and 4.0 wt%, which correspond to P_{sat} of 6.2 MPa and 10.3 MPa, respectively [56]. Fig. 7(a) and (b) shows that at a low CO_2 concentration (i.e., 2.3 wt%), increasing the talc content from 0.5 to 5.0 wt% advanced the onset time of cell nucleation and increased the cell density. More importantly, Fig. 8(a) and (b) provides further evidence of the enhancement of bubble formation around the expanding bubbles, especially when talc particles were present. With higher talc content (Fig. 8b), the number of tiny bubbles formed around the expanding cells increased significantly. These results suggest that the extensional stress-induced nucleation became more pronounced as talc content increased.

As Fig. 9(a) and (b) illustrates, when the dissolved CO_2 content was increased to 4.0 wt%, the onset time of cell formation only slightly advanced, while cell density was virtually invariant when the talc content was increased from 0.5 to 5.0 wt%. These results, consistent with the results of earlier studies using extrusion foaming [18,20], revealed that the effect of higher talc content on cell density of PS–CO_2 foaming was negligible when the CO_2 content was high. A more detailed explanation will be provided in Section 4.3, which discusses the effect of gas content on the phenomena.

4.3. Effect of gas content on cell nucleation

Regardless of the talc content, the *in situ* visualization data shown in Figs. 7(a) and 9(a), as well as Figs. 7(b) and 9(b), show that the onset time of bubble formation advanced and the cell density increased significantly when the CO_2 content increased from 2.3 wt% to 4.0 wt%. On the one hand, the higher CO_2 content increased the abundance of CO_2 molecules to form gas cavities. On the other hand, it reduced γ_{lg} [57] and resulted in decreases in R_{cr}, W_{hom}, and W_{het}. These consequences, in turn, increased the nucleation rate of new cells and enhanced the growth activation of the pre-existing gas cavities. Furthermore, as shown in Fig. 10(a) and (b), there was virtually no trace of the extensional-stress induced nucleation in either sample foamed at the higher CO_2 concentration, suggesting that the pressure fluctuation may not be significant when the CO_2 content was high. Dissolving a larger amount of CO_2 in the PS promoted the plasticizing effect and reduced the viscosity

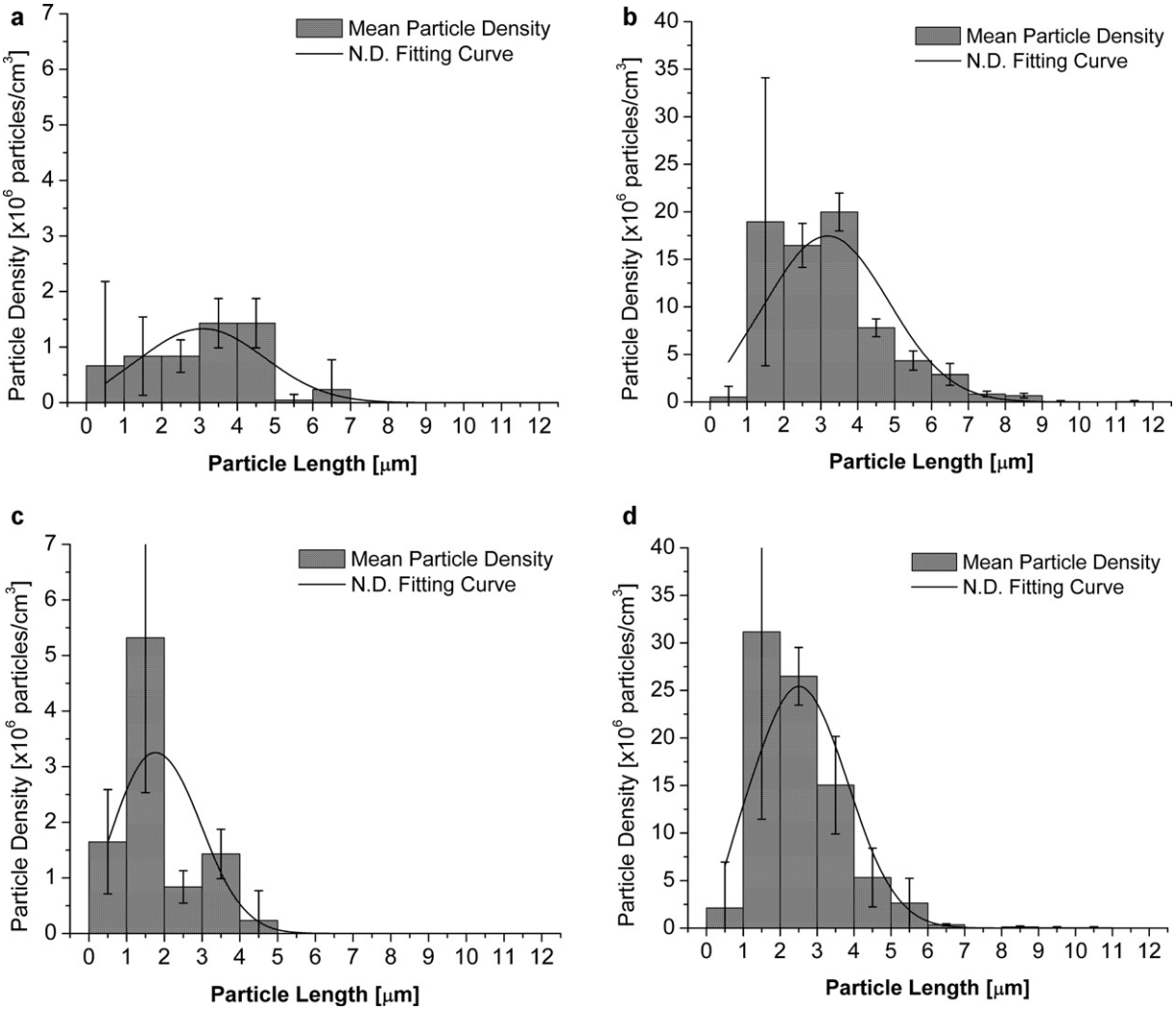

Fig. 13. Distribution of talc particle sizes in PS–talc composites: (a) 0.5 wt% of untreated talc; (b) 5.0 wt% of untreated talc; (c) 0.5 wt% of surface-treated talc; and (d) 5.0 wt% of surface treated talc. (a) Mean size = 3.10 μm and std. dev. = 1.55 μm; (b) mean size = 1.76 μm and std. dev. = 1.00 μm; (c) mean size = 3.10 μm and std. dev. = 1.55 μm; (d) mean size = 2.55 μm and std. dev. = 1.20 μm.

and elasticity of the PS–CO_2 solution. Gendron and Champagne [58] found that the level of plasticization observed for CO_2 and ethanol are approximately the same (i.e., −8 °C/wt%). In other words, the mobility of the fluid increased. It is believed that the increase in the fluidity of the PS–CO_2 solution would reduce the potential extensional stress field that would be established near the PS–talc interface. This would suppress the induction of the negative ΔP_{local} around the talc aggregates and led to the lack of noticeable effects of increasing talc content on cell density. Nonetheless, additional theoretical studies on the effect of viscosity and elasticity of the polymer–gas mixture on stress distribution around the inorganic filler particles are needed to verify this speculation.

4.4. Effect of surface treatment on cell nucleation

The foaming behavior of PS–talc samples with surface-treated talc particles (CB7) was studied and compared with that of PS–talc samples with talc particles without surface treatment (CIMPACT 710) to examine the effect of surface treatment on the cell nucleation behaviors. Both samples consisted of 5 wt% of talc and were saturated with 2.3 wt% of CO_2 at 180 °C with similar pressure drop profiles. Fig. 11(a) illustrates the micrographs of the *in situ* foaming processes of the samples with the surface-treated talc. In a comparison of the visualization data for surface-treated and untreated talc (i.e., Fig. 7b), it becomes clear that the onset time of cell nucleation and the cell density were virtually invariant in the two cases. Moreover, as Fig. 11(b) indicates, in both cases the growth of nucleated cells promoted the nucleation of new cells around them. However, the phenomenon was slightly less pronounced in the case of the surface-treated talc (i.e., Fig. 8b). Since the surface treatment is believed to affect the compatibility and thereby the bonding between PS and talc, it is surmised that the treatment has an effect on the establishment of the stress field.

Unfortunately, the type of surface treatment was considered confidential information by the supplier and was not available to us. Therefore, a series of scanning electron microscopy (SEM) pictures were taken of the unfoamed PS–talc samples to analyze the effects of the surface treatment on the size distribution of talc particles. A sample SEM micrograph is illustrated in Fig. 12, which shows an even distribution of talc particles in the PS matrix. The distributions of the talc particle sizes (i.e., the length of the largest dimension) for varying loadings and surface treatments are illustrated in Fig. 13(a)–(d). The analyzed data reveal that the surface treatment on the talc particles improved the compatibility between PS and talc. The results were consistent with those of Alonso et al. [59]. As a result, it enhanced the dispersion of talc particles within

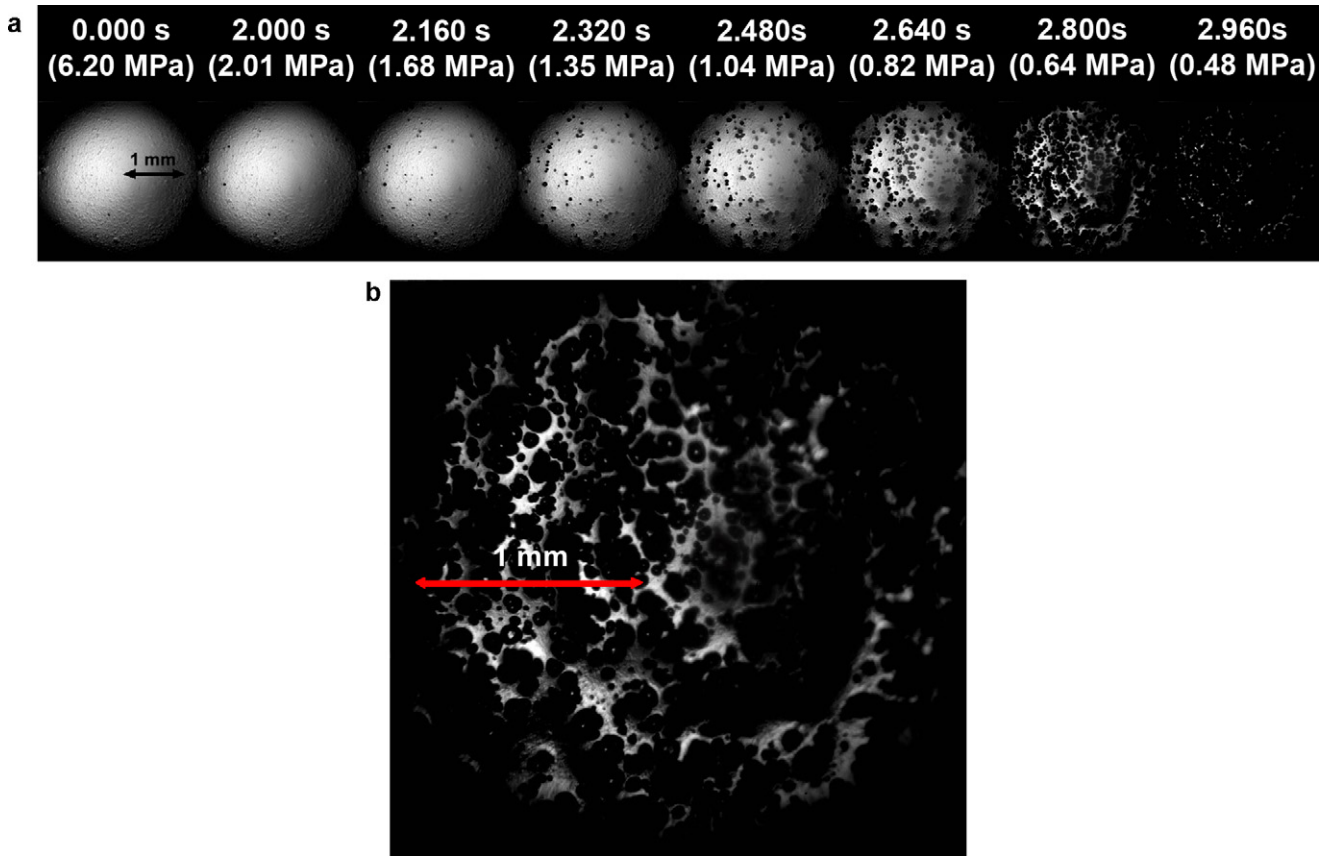

Fig. 14. Micrographs of PS + 5.0 wt% talc (STELLAR 410) with 2.3 wt% CO_2 at 180 °C: (a) until 2.96 s (0.48 MPa) and (b) at 2.82 s (0.62 MPa).

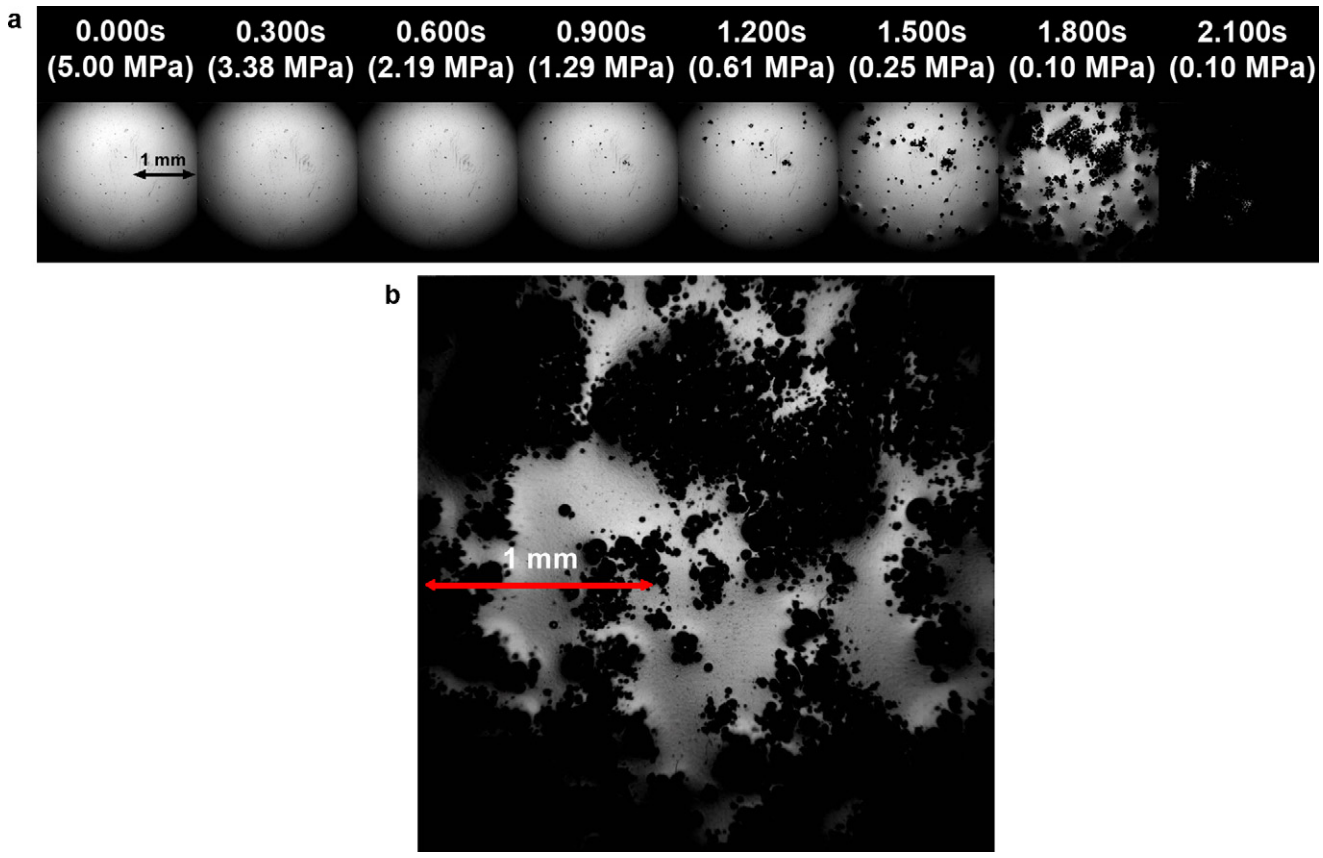

Fig. 15. Micrographs of PS + 5.0 wt% talc (CIMPACT 710) with 2.1 wt% CO_2 at 140 °C: (a) until 2.10 s (0.10 MPa) and (b) at 1.900 s (0.10 MPa).

the PS matrix and resulted in a smaller mean particle size and lower standard deviation. It is believed that the improved compatibility between PS and talc particles would lead to a smaller amount of trapped CO_2 cavities. Moreover, the increased compatibility between the polymer and the talc particles would increase the wettability of the polymer on the talc surface, thereby reducing the size of θ_c and increasing W_{het}. As a result, although the improved dispersion of talc particles due to their surface treatment increased the total surface area of the PS–talc interfaces, the stress-enhanced nucleation of new cells by the expanding bubbles became less pronounced.

4.5. Effects of talc particle size on cell nucleation

The effect of talc particle size on cell nucleation was investigated by observing the foaming behavior of a PS–talc sample with larger talc particles (i.e., STELLAR 410) and comparing the observed foaming phenomena to those obtained with smaller talc particles. Both samples used 5 wt% of talc loadings, and they were saturated with 2.3 wt% of CO_2 at 180 °C before depressurizing. Fig. 14(a) illustrates the micrographs of the *in situ* foaming process of the sample with the larger talc particles. A comparison of the extracted micrographs of both experiments (i.e., Fig. 7b) shows that the onset time of cell nucleation and the cell density were virtually unaffected by the mean size of talc particles. Since the larger particles would create a smaller total surface area of the PS–talc interface as well as a smaller number of particles, cell nucleation was expected to be suppressed with the use of larger particles (see Eq. (9)). However, observations showed that the particle size did not influence the cell density. One possible explanation was that larger talc particles would lead to a higher degree of local pressure variation (i.e., ΔP_{local} in Eq. (13)), enhancing cell nucleation or formation. Further studies will be needed to clarify the effects of talc particle size on local stress distribution and the cell nucleation mechanism.

4.6. Effect of processing temperature on cell nucleation

In order to explore the effect of the processing temperature on the heterogeneous nucleation mechanism induced by the presence of inorganic fillers, a PS–talc sample with 5 wt% of talc loading (CIMPACT 710) was saturated with 2.1 wt% of CO_2 at a pressure of 5.0 MPa [56] and set at a lower system temperature (i.e., 140 °C). The experimental results were compared with those obtained at a system temperature of 180 °C (i.e., Figs. 3b and 4b). Both experiments were conducted by rapidly depressurizing the chamber with similar pressure drop profiles. Fig. 15(a) illustrates the *in situ* foaming phenomena at the lower processing temperature. Consistent with our previous studies [60,61], the onset time of cell nucleation was delayed and cell density was increased by lowering the foaming temperature. The later onset time of cell nucleation at the lower processing temperature was a result of the higher free energy barrier and the larger R_{cr} caused by the higher γ_{lg} [57]. Meanwhile, the lower gas diffusivity suppressed excessive cell growth. With a larger portion of gas contributed to the nucleation of new cells, it resulted in a higher cell density. Furthermore, Fig. 15(b), when compared to Fig. 4(b), clearly indicates that the number of smaller cells formed around the expanding cells increased substantially when the system temperature was reduced from 180 °C to 140 °C. Reduction of the processing temperature would increase both the viscosity and the elasticity of the polymer–gas solution. It is believed that the restricted fluid mobility would enhance the establishment of extensional stress (i.e., $\Delta P_{local} < 0$ in Eq. (13)) on the side surfaces of the talc aggregates, and thereby R_{cr}, W_{hom}, and W_{he} would be reduced. Therefore, the extensional stress-induced nucleation around the expanding bubbles would become more significant at lower temperatures. However, a further investigation will be helpful to verify the relationships among viscosity, elasticity, and the stress distribution around the polymer–filler interfaces during an extensional flow.

5. Conclusions

The addition of cell nucleating agents in polymer is a common way to enhance cell nucleation in foaming plastics. It is widely believed that enhancement will result from a lower free energy barrier which initiates heterogeneous nucleation. From these experimental results, it is deduced that the heterogeneous nucleation mechanism, with the presence of nucleating agents, is closely related to local pressure fluctuations around the polymer–nucleating agent interface. These results could be explained by the numerical simulation conducted by Wang et al. [32], which suggested the growing cells would generate extensional stress fields the presence of talc particles. Such extensional stress field would result in a further pressure reduction and a higher degree of supersaturation in the local regions. Consequently, R_{cr}, W_{hom}, and W_{het} for bubble nucleation would decrease, promoting the nucleation of new cells, or the growth of pre-existing gas cavities. At higher gas content, the reduction of viscosity and elasticity of the polymer–gas solution might weaken the extensional stress field being generated and suppress additional reduction of the local pressure. This might potentially explain the limited impact of increasing talc content on cell density with a higher CO_2 content [18,20]. Finally, the study observed that lower processing temperature and higher talc content promoted stress-induced nucleation, whereas improved PS–talc compatibility slightly reduced it. However, the size of talc seemed to have no significant effect on the phenomenon.

Acknowledgment

The authors are grateful to the Consortium for Cellular and Micro-Cellular Plastics (CCMCP), Auto21, and NSERC for the financial supports of this project.

References

[1] C.B. Park, N.P. Suh, Rapid heating for microcellular nucleation in a polymer melt, in: Proceedings of Society of Polymer Engineering Annual Technical Conference, Technical Papers Proceedings, Detroit, 1992, p. 1513.
[2] L.M. Matuana, C.B. Park, J.J. Balatinecz, Cell morphology and property relationships of microcellular foamed pvc/wood-fiber composites, Polymer Engineering and Science 38 (1998) 1862–1872.
[3] M. Shimbo, I. Higashitani, Y.J. Miyano, Mechanism of strength improvement of foamed plastics having fine cells, Journal of Cellular Plastics 43 (2007) 157–167.
[4] M. Michaeli, L. Florez, Improving of impact behaviour of structural foams, in: Proceedings of Blowing Agents and Foaming Processes Conference, Hamburg, Germany, 2009.
[5] K.A. Seeler, V. Kumar, Tension-tension fatigue of microcellular polycarbonate: initial results, Journal of Reinforced Plastics and Composites 12 (1993) 359–376.
[6] L. Glicksman, Notes from MIT Summer Ptorgram 4.10 S Foams and Cellular Materials: Thermal and Mechanical Properties, Cambridge, MA, June 29–July 1, 1992.
[7] K.W. Suh, C.P. Park, J.J. Maurer, M.H. Tusim, R.D. Genova, R. Broos, D.P. Sophiea, Lightweight cellular plastics, Advanced Materials 12 (2000) 1779–1789.
[8] A. Kabumoto, N. Yoshida, M. Itoh, M. Okada, Light reflection plate, U.S. Patent 5,844,731, 1998.
[9] R.H. Hansen, W.M. Martin, Novel methods for the production of foamed polymers. Nucleation of dissolved gas by localized hot spots, Industrial and Engineering Chemistry Product Research and Development 3 (1964) 137–141.
[10] R.H. Hansen, W.M. Martin, Novel methods for the production of foamed polymers. ii. Nucleation of dissolved gas by finely divided metals, Journal of Polymer Science Part B: Polymer Letters 3 (1965) 325–330.
[11] H.H. Yang, C.D. Han, The effect of nucleating agents on the foam extrusion characteristics, Journal of Applied Polymer Science 29 (1984) 4465–4470.
[12] F.N. Wilkenlog, P.A. Wilson, S.A. Fox, Coating electrically conductive wire with polyolefin, U.S. Patent 4,107,354, 1978.
[13] C.D. Han, Y.W. Kim, K.D. Malhotra, A study of foam extrusion using a chemical blowing agent, Journal of Applied Polymer Science 20 (1976) 1583–1596.
[14] H.A. Ehrenfruend, Method of making polyethylene foam, U.S. Patent 4,110,269, 1978.

[15] C.Y. Ma, C.D. Han, Foam extrusion characteristics of thermoplastic resin with fluorocarbon blowing agent. II: Polystyrene foam extrusion, Journal of Applied Polymer Science 28 (1983) 2983–2998.
[16] J.S. Colton, N.P. Suh, The nucleation of microcellular thermoplastic foam with additives. Part II: experimental results and discussion, Polymer Engineering and Science 27 (1987) 493–499.
[17] R.B. Allen, R.W. Avakian, Foamable polycarbonate compositions, articles and methods, U.S. Patent 4,544,677, 1985.
[18] C.B. Park, L.K. Cheung, S.W. Song, The effect of talc on cell nucleation in extrusion foam processing of polypropylene with CO_2 and isopentane, Cellular Polymers 17 (1998) 221–251.
[19] H.E. Naguib, C.B. Park, P.C. Lee, Effect of talc content on the volume expansion ratio of extruded PP foams, Journal of Cellular Plastics 39 (2003) 499–511.
[20] X. Xu, C.B. Park, D. Xu, R. Pop-Iliev, Effects of die geometry on cell nucleation of PS foams blown with CO_2, Polymer Engineering and Science 43 (2003) 1378–1390.
[21] P.H. Nam, P. Maiti, M. Okamoto, T. Kotaka, T. Nakayama, M. Takada, Foam processing and cellular structure of polypropylene/clay nanocomposites, Polymer Engineering and Science 42 (2002) 1907–1918.
[22] Y.H. Lee, C.B. Park, K.H. Wang, M.H. Lee, HDPE/clay nanocomposite foams blown with supercritical CO_2, Journal of Cellular Plastics 41 (2005) 487–502.
[23] K. Taki, T. Yanagimoto, E. Funami, M. Ohshima, Visual observation of CO_2 foaming of polypropylene-clay nanocomposites, Polymer Engineering and Science 44 (2004) 1004–1011.
[24] M.J. Yuan, L.S. Turng, Microstructure and mechanical properties of microcellular injection molded polyamide-6 nanocomposites, Polymer 46 (2005) 7273–7292.
[25] J. Shen, C. Zeng, J. Lee, Synthesis of polystyrene-carbon nanofibers nanocomposite foams, Polymer 46 (2005) 5218–5224.
[26] X. Han, C. Zeng, L.J. Lee, K.W. Koelling, D.L. Tomasko, Extrusion of polystyrene nanocomposite foams with supercritical CO_2, Polymer Engineering and Science 43 (2003) 1261–1275.
[27] D.L. Tomasko, X. Han, D. Liu, W. Gao, Supercritical fluid applications in polymer nanocomposites, Current Opinion in Solid State and Material Science 7 (2003) 407–412.
[28] D. Turnbull, B. Vonnegut, Nucleation catalysis, Industrial and Engineering Chemistry 44 (1952) 1292–1298.
[29] N.H. Fletcher, Size effect in heterogeneous nucleation, Journal of Chemical Physics 29 (1958) 572–576.
[30] R. Cole, Boiling Nucleation, Advances in Heat Transfer 10 (1974) 85–166.
[31] S.N. Leung, A. Wong, C.B. Park, J.H. Zong, Ideal surface geometry of nucleating agents to enhance cell nucleation in polymer foaming, Journal of Applied Polymer Science 108 (2008) 3997–4003.
[32] C. Wang, S.N. Leung, M. Bussmann, W.T. Zhai, C.B. Park, Numerical investigation of nucleating-agent-enhanced heterogeneous nucleation, Industrial and Engineering Chemistry Research 49 (2010) 12783–12792.
[33] S.T. Lee, Shear effects on thermoplastic foam nucleation, Polymer Engineering and Science 33 (1993) 418–422.
[34] C.D. Han, C.A. Villamizar, Studies on structural foam processing. I: The rheology of foam extrusion, Polymer Engineering and Science 18 (1978) 687–698.
[35] J.H. Han, C.D. Han, A study of bubble nucleation in a mixture of molten polymer and volatile liquid in a shear flow field, Polymer Engineering and Science 28 (1988) 1616–1627.
[36] K. Taki, T. Nakayama, T. Yatsuzuka, M. Ohshima, Visual observations of batch and continuous foaming processes, Journal of Cellular Plastics 39 (2003) 155–169.
[37] J. Tatibouët, R. Gendron, A study of strain-induced nucleation in thermoplastic foam extrusion, Journal of Cellular plastics 40 (2004) 27–44.
[38] L. Chen, H. Sheth, X. Wang, Effects of shear stress and pressure drop rate on microcellular foaming process, Journal of Cellular Plastics 37 (2001) 353–363.
[39] W. Zhu, N. Zhou, J. Qu, W. Xu, L.J. Kong, Effects of mechanical vibration on cell density and cell morphology in the dynamic microcellular foaming process, Journal of Cellular Plastics 42 (2006) 49–61.
[40] C.Y. Gao, N.Q. Zhou, X.F. Peng, P. Zhang, Optimized polystyrene cell morphology by orthogonal superposition of oscillatory shear, Polymer-Plastics Technology and Engineering 45 (2006) 1025–1029.
[41] A. Wong, R.K.M. Chu, S.N. Leung, C.B. Park, J.H. Zong, A batch foaming visualization system with extensional stress-inducing ability, Chemical Engineering Science 66 (2011) 55–63.
[42] Q. Guo, J. Wang, C.B. Park, M.A. Ohshima, A microcellular foaming simulation system with a high-pressure drop rate, Industrial and Engineering Chemistry Research 45 (2006) 6153–6161.
[43] J.W. Gibbs, The Scientific Papers of J. Willard Gibbs, Volume 1, Dover, New York, 1961.
[44] A.S. Tucker, C.A. Ward, Critical state of bubbles in liquid–gas solutions, Journal of Applied Physics 46 (1975) 4801–4808.
[45] S.N. Leung, A. Wong, Q. Guo, C.B. Park, J.H. Zong, Change in the critical nucleation radius and its impact on cell stability during polymeric foaming processes, Chemical Engineering Science 64 (2009) 4899–4907.
[46] C.A. Ward, E. Levart, Conditions for stability of bubble nuclei in solid surfaces contacting a liquid–gas solution, Journal of Applied Physics 56 (1984) 491–500.
[47] C.A. Ward, A. Balakrishnan, F.C. Hooper, On the thermodynamics of nucleation in weak liquid-gas solutions, Transactions of the ASME Series D: Journal of Basic Engineering 92 (1970) 695–704.
[48] E.N. Harvey, D.K. Barnes, W.D. McElroy, A.H. Whiteley, D.C. Pease, K.W. Cooper, Journal of Cellular and Comparative Physiology 24 (1944) 1–22.
[49] M. Blander, Bubble nucleation in liquids, Advances in Colloid and Interface Science 10 (1979) 1–32.
[50] P.M. Wilt, Nucleation rates and bubble stability in water-carbon dioxide solutions, Journal of Colloid and Interface Science 112 (1986) 530–538.
[51] M. Blander, J.L. Katz, Bubble nucleation in liquids, AIChE Journal 21 (1975) 833–848.
[52] S.N. Leung, C.B. Park, H. Li, Numerical simulation of polymeric foaming processes using a modified nucleation theory, Plastics, Rubber and Composites: Macromolecular Engineering 35 (2006) 93–100.
[53] S. Levy, Advances in Plastics Technology, Van Nostrand Reinhold, New York, 1981.
[54] J.H. Han, C.D. Han, Bubble nucleation in polymeric liquids. II: Theoretical considerations, Journal of Polymer Science Part B: Polymer Physics 28 (1990) 743–761.
[55] J.H. Saunders, Referring to a chapter in a book, in: D. Klempner, K.C. Frisch (Eds.), Handbook of Polymeric Foams and Foam Technology, Hanser Publishers, New York, 1991, pp. 5–14.
[56] G. Li, J. Wang, C.B. Park, P. Moulinie, R. Simha, Comparison of the SS-based and SL-based estimation of gas solubility, in: Proceedings of Society of Polymer Engineering Annual Technical Conference, Technical Papers Proceedings, Detroit, 2004, p. 2566.
[57] H. Park, C.B. Park, C. Tzoganakis, K.H. Tan, P. Chen, Surface tension measurement of polystyrene melts in supercritical carbon dioxide, Industrial and Engineering Chemistry Research 45 (2006) 1650–1658.
[58] R. Gendron, M.F. Champagne, Foaming polystyrene with a mixture of CO_2 and ethanol, Journal of Cellular Plastics 42 (2006) 127–138.
[59] M. Alonso, I. Velasco, J.A. de Saja, Constrained crystallization and activity of filler in surface modified talc polypropylene composites, European Polymer Journal 33 (1997) 255–262.
[60] A. Wong, S.N. Leung, G.Y.G. Li, C.B. Park, Role of processing temperature in polystyrene and polycarbonate foaming with carbon dioxide, Industrial and Engineering Chemistry Research 46 (2007) 7107–7116.
[61] S.N. Leung, A. Wong, C.B. Park, Q. Guo, Strategies to estimate the pressure drop threshold of nucleation for polystyrene foam with carbon dioxide, Industrial and Engineering Chemistry Research 48 (2009) 1921–1927.